Eddy compensation and controls of the enhanced sea-to-air CO 2 flux during positive phases of the Southern Annular Mode

Carolina Dufour, Julien Le Sommer, Marion Gehlen, James Orr, Jean-marc Molines, Jennifer Simeon, Bernard Barnier

GLOBAL BIOGEOCHEMICAL CYCLES, VOL. 27, 950–961, doi:10.1002/gbc.20090, 2013

Eddy compensation and controls of the enhanced sea-to-air CO_2 flux during positive phases of the Southern Annular Mode

Carolina O. Dufour,[1,2] Julien Le Sommer,[3] Marion Gehlen,[2] James C. Orr,[2] Jean-Marc Molines,[3] Jennifer Simeon,[2] and Bernard Barnier[3]

Received 1 November 2012; revised 3 September 2013; accepted 9 September 2013; published 23 September 2013.

[1] The current positive trend in the Southern Annular Mode (SAM) is thought to reduce the growth rate of the Southern Ocean CO_2 sink because enhanced wind-driven upwelling of dissolved inorganic carbon (DIC) increases outgassing of natural CO_2. However, no study to date has quantified the potentially large role of mesoscale eddies in compensating intensified upwelling nor the mixed-layer processes in terms of their effects on CO_2 fluxes. Here we report on results from two new simulations in a regional 0.5° eddying model of the Southern Ocean. The first simulation is forced with interannually varying atmospheric reanalysis and coupled to a biogeochemistry model run under constant preindustrial atmospheric CO_2. The second simulation is like the first except that superimposed on the forcing is a poleward shifted and intensified westerlies wind anomaly consistent with the positive phase of the SAM. In response to the SAM, the Southern Ocean's sea-to-air CO_2 flux is enhanced by 0.1 Pg C yr^{-1} per standard deviation of the SAM, mostly from the Antarctic Zone (AZ), where enhanced surface DIC is only partly compensated by enhanced surface alkalinity. Increased mixed-layer DIC in the AZ results from a combination of increased upwelling below the mixed layer and increased vertical diffusion at the base of the mixed layer. Previous studies overlooked the latter. Thus, upward supply of DIC and alkalinity depends on associated vertical gradients just below the mixed layer, which are affected by interior ocean transport. Our eddying model study suggests that about one third of the SAM enhancement of the Ekman-induced northward DIC transport is compensated by southward transport from standing and transient eddies.

Citation: Dufour, C. O., J. Le Sommer, M. Gehlen, J. C. Orr, J.-M. Molines, J. Simeon, and B. Barnier (2013), Eddy compensation and controls of the enhanced sea-to-air CO_2 flux during positive phases of the Southern Annular Mode, *Global Biogeochem. Cycles*, *27*, 950–961, doi:10.1002/gbc.20090.

1. Introduction

[2] The Southern Ocean is a sink of anthropogenic CO_2, accounting for about 40% of total ocean uptake while covering only 25% of the global ocean area [*Orr et al.*, 2001; *Sarmiento et al.*, 1992; *Sabine et al.*, 2004; *Mikaloff-Fletcher et al.*, 2006; *Gruber et al.*, 2009]. The Southern Ocean CO_2 sink is expected to track the increase in atmospheric CO_2, but modeling studies that account for trends in climate forcing suggest that its growth rate has fallen off that of atmospheric CO_2 since the 1980s [*Wetzel et al.*, 2005; *Le Quéré et al.*, 2007; *Lovenduski et al.*, 2008; *Lenton et al.*, 2009; *Le Quéré et al.*, 2010; *Takahashi et al.*, 2012]. The cause appears to be the trend toward more positive phases of the Southern Annular Mode (SAM), a tendency that is detectable in both observations and models [*Marshall*, 2003; *Sen Gupta and England*, 2006] and attributed to anthropogenic forcing [*Marshall et al.*, 2004; *Lenton et al.*, 2009]. This trend is expected to persist over the remainder of the 21st century [*Thompson et al.*, 2011].

[3] The SAM is the dominant mode of atmospheric variability in the Southern Hemisphere. Its positive phases are associated with an intensification and a poleward shift of the surface westerlies [*Sen Gupta and England*, 2006]. Previous work suggests that positive phases of the SAM result in stronger upwelling of DIC-rich water at the Antarctic Divergence, bringing more DIC to the surface, part of which is lost to the atmosphere as CO_2 [*Le Quéré et al.*, 2007; *Lovenduski et al.*, 2007; *Lenton and Matear*, 2007]. Enhanced outgassing of natural CO_2 due to the positive trend in the SAM

Additional supporting information may be found in the online version of this article.

[1]Laboratoire des Ecoulements Géophysiques et Industriels, CNRS-Université de Grenoble, Grenoble, France.
[2]LSCE/IPSL, Laboratoire des Sciences du Climat et l'Environnement, CEA-CNRS-UVSQ, Gif-sur-Yvette, France.
[3]Laboratoire de Glaciologie et Géophysique de l'Environnement, CNRS-Université de Grenoble, Grenoble, France.

Corresponding author: C. O. Dufour, Program in Atmospheric and Ocean Sciences, Princeton University, Princeton, NJ, USA. (cdufour@princeton.edu)

0886-6236/13/10.1002/gbc.20090

would thus compete against the increasing anthropogenic CO_2 uptake, reducing the growth rate of the Southern Ocean CO_2 sink.

[4] Conversely, an observational study [*Böning et al.*, 2008] found no detectable increase in the slope of isopycnal surfaces despite the trend in westerlies, thus suggesting that the meridional overturning circulation (MOC) would be insensitive to the SAM. Eddying model studies support this conclusion, because eddy fluxes tend to better compensate the wind-induced increase in Ekman transport as model resolution increases, thus reducing the sensitivity of the MOC to the SAM [*Hallberg and Gnanadesikan*, 2006; *Farneti et al.*, 2010; *Spence et al.*, 2010; *Dufour et al.*, 2012]. Thus, non-eddying models may well overestimate the response of CO_2 fluxes to the SAM.

[5] Recent results from eddying circulation models hint at partial compensation, but results are mixed: The Antarctic Circumpolar Current (ACC) transport's sensitivity to wind increase is nearly compensated by eddy fluxes, whereas the enhanced Meridional Overturning Circulation (MOC) transport is only partially compensated [*Meredith et al.*, 2012; *Dufour et al.*, 2012; *Morrison and Hogg*, 2013]. Yet no eddying model study has quantified the extent to which eddy fluxes may reduce the enhanced outgassing of natural CO_2 fluxes due to the SAM. Hence, the response of CO_2 flux to the positive trend in the SAM remains an open question that can be addressed by eddying models.

[6] Previous studies with coarse-resolution models found that the SAM-induced increase in surface DIC is mostly driven by physical processes, while the role of biological processes is negligible [*Le Quéré et al.*, 2007; *Lovenduski et al.*, 2007; *Lenton and Matear*, 2007]. Those studies proposed that the increase in surface DIC is caused mainly by enhanced upwelling from a stronger MOC, but they did not assess other physical processes that may also contribute. More recently, a coarse-resolution model study suggests that diapycnal mixing may also contribute to increasing surface DIC [*Lovenduski et al.*, 2013].

[7] We made simulations with a regional circulation model of the Southern Ocean that begins to explicitly resolve large mesoscale features. Its resolution is higher than those used in previous studies, but it remains a first step into the eddying regime because it does not resolve the full eddy energy spectrum. In particular, its finer bathymetry allows a refined spatial representation of the response of sea-air CO_2 flux to the SAM.

2. Methods

2.1. Models

[8] In this study, we use the ocean modeling framework known as the *Nucleus for European Modeling of the Ocean* (NEMO) [*Madec*, 2008]. NEMO couples three components: the oceanic circulation model *Ocean Parallélisé* [*Madec et al.*, 1998], a hydrostatic primitive equation ocean model with a free surface using a nonlinear equation of state, the Louvain-la-Neuve sea Ice Model [*Fichefet and Maqueda*, 1997], a multi-layer dynamic and thermodynamic model of sea ice, and the Pelagic Interaction Scheme for Carbon and Ecosystem Studies ocean biogeochemistry model (PISCES) [*Aumont and Bopp*, 2006], a model with 24 compartments simulating the biogeochemical cycles of carbon and nutrients. Model simulations are forced by the DRAKKAR Forcing Set 3 [*Brodeau et al.*, 2010] that combines forcing products from the European Centre for Medium-Range Weather Forecasts (ECMWF) Reanalysis (ERA-40, until year 2001) and the ECMWF analysis (from 2002 up to 2004, for air temperature, humidity, and 10 m winds) and satellite observations (for precipitation and radiation).

[9] The model configuration belongs to a hierarchy of model configurations developed within the DRAKKAR high-resolution ocean modeling consortium [*Drakkar Group*, 2007]. Here we use a regional configuration identical to the DRAKKAR global model ORCA05, south of 30°S. It has a nominal horizontal resolution of 0.5° on a Mercator grid, but its latitudinal spacing varies with the cosine of latitude. Thus, at 60°S, the grid size is 28 km. The vertical grid has 46 levels with the finest thickness (6 m) at the near surface to better capture mixed-layer processes, where layer thickness gradually increases with depth to 250 m for the deepest level. The complete model configuration is called *BIOPERIANT05*, where *BIO* signifies that the PISCES model is included and *PERIANT05* refers to the physical model configuration described in *Dufour et al.* [2012]. Antarctic Bottom Water properties are relaxed toward the temperature and salinity climatology of *Gouretski and Koltermann* [2004] in order to maintain their observed structure. To avoid an excessive model drift, surface salinity is relaxed toward the *Levitus et al.* [1998] climatology with a restoring time of 600 days over the top 50 m [*Griffies et al.*, 2009]. Vertical mixing is represented by a Turbulent Kinetic Energy scheme and a background vertical mixing coefficient of 10^{-5} m^2 s^{-1} with enhanced mixing in case of static instability [*Madec*, 2008]. Following *Lachkar et al.* [2007, 2009a, 2009b], who use the global version of the model at the same resolution (ORCA05), we do not use an eddy-transport parameterization, such as that of *Gent and McWilliams* [1990]. That allows eddies to be explicitly, although only partly, resolved by the model. Sea-air CO_2 fluxes are computed following the classic approach:

$$F = k \cdot \alpha \cdot \left(pCO_2{}^{oc} - pCO_2{}^{atm}\right)(1 - f_{ice}) \quad (1)$$

where k is the gas transfer coefficient, α is the CO_2 solubility, $pCO_2{}^{oc}$ and $pCO_2{}^{atm}$ are the partial pressures of CO_2 in the ocean and atmosphere, and f_{ice} is the sea ice fraction. The coefficient k varies with wind speed following *Wanninkhof* [1992, equation (3)], and α is computed from *Weiss and Price* [1980].

2.2. Simulations

[10] The physical model, including ocean and sea ice, is initialized in year 1977 from the output of a previous simulation of PERIANT05 run from 1958 to 1976. Biogeochemical variables are initialized from the World Ocean Atlas 2001 [*Conkright et al.*, 2002] and from annual fields of Global Ocean Data Analysis Project (GLODAP) [*Key et al.*, 2004] with DIC corrected to preindustrial conditions (see supporting information).

[11] Simulations are run under preindustrial atmospheric CO_2, using a constant mixing ratio of 278 ppm [*Barnola et al.*, 1987]. With this modeling framework, we made two simulations: a control experiment (REF05) where the model is forced with atmospheric reanalysis winds, and a sensitivity experiment ($SAM05^{+++}$) where winds are perturbed

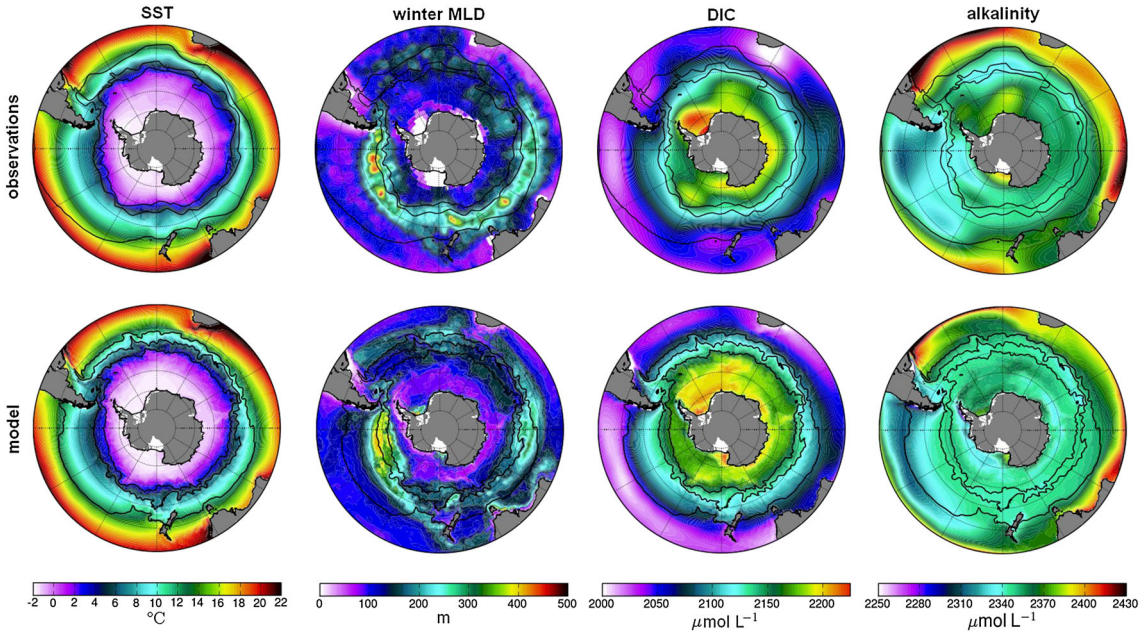

Figure 1. (Top) Data-based climatologies of sea surface temperature (SST) [*Hurrell et al.*, 2008], winter (July–August–September) mixed-layer depth [*De Boyer Montégut et al.*, 2004], and surface preindustrial DIC and surface alkalinity from GLODAP [*Key et al.*, 2004] compared to (bottom) corresponding simulated results for the 1995–2004 mean from REF05. For comparison, climatologies were regridded to the 0.5° model grid. The mixed-layer depth is computed using the same density-difference criterion ($\Delta\sigma \leq 0.03$ kg m^{-3}) for both model and observations. Black contours indicate mean STF, SAF, and PF positions computed from (top) *Orsi et al.* [1995] and (bottom) REF05 following *Sallée et al.* [2008].

according to positive phases of the SAM. For SAM05^{+++}, an anomaly of wind velocity corresponding to +2 standard deviations of the SAM index over 1980–2001 was added permanently to the basic forcing (see supporting information and *Dufour et al.* [2012] who use the same experiments and names). This approach offers two benefits: (i) it accumulates the effect of positive phases of the SAM over several decades, thereby revealing the long-term response of the ocean to the SAM, and (ii) it provides a strong response of the ocean to the SAM that can be easily distinguished from the ocean's intrinsic variability.

2.3. Diagnostics

[12] The Southern Ocean is separated into four regions, each with rather homogeneous physical and biogeochemical properties, with those being delimited by three major fronts: the Subtropical Front (STF), the Subantarctic Front (SAF), and the Polar Front (PF). Most of the subsequent diagnostics focus on the four interfrontal regions: the Subtropical Zone (*STZ*, north of the STF), the Subantarctic Zone (*SAZ*, between the SAF and STF), the Polar Front Zone (*PFZ*, between the PF and SAF), and the Antarctic Zone (*AZ*, south of the PF). Mean front positions are computed from annual mean model output. The STF is defined as the mean 10°C isotherm at 150 m following *Orsi et al.* [1995]. The SAF and PF are defined using a method comparable to that of *Sallée et al.* [2008]. Both are computed from the surface dynamic height anomaly referenced to 1500 m, where the PF corresponds to the 0.95 m anomaly and the SAF to the 1.20 m anomaly as in *Dufour et al.* [2011].

[13] In this study, the model's response to the SAM is computed as the difference between SAM05^{+++} and REF05 simulations. For integrated quantities, this response is presented in terms of an anomaly per standard deviation of the SAM, as indicated by std^{-1}(SAM). To limit boundary effects in spatial integrals, the northern boundary is taken to be 31°S. Analyses are carried out over 1995–2004, the last 10 years of simulation, after a spin-up of the circulation from 1958 to 1976 followed by further spin-up with the fully coupled PISCES model over 1977–1994. We use the convention where positive values indicate a CO_2 flux from sea to air: positive refers to ocean outgassing while negative values refers to ocean uptake of natural carbon.

3. Results

3.1. Model Evaluation

[14] The 1995–2004 averaged transport at Drake Passage of the simulation REF05 is 142 Sv, which falls within the observed range of 110 to 150 Sv [*Whitworth*, 1983; *Cunningham et al.*, 2003]. In REF05, the 1995–2004 averaged MOC in potential density has a maximum value of 8 Sv in the subpolar cell. This cell corresponds to the North Atlantic Deep Water (NADW) that moves southward, upwells at roughly 55°S, is transformed into Antarctic Intermediate Water (AAIW), and flows back to the north. The subpolar cell in REF05 is less intense than data-based estimates of *Talley* [2003] (15–20 Sv), but it is within the range simulated by other models (8–18 Sv) [e.g., *Hallberg and Gnanadesikan*, 2006; *Lenton and Matear*, 2007]. The mean state and response to the SAM for both ACC and MOC transport are similar to those in a previous version of the same model [*Dufour et al.*, 2012].

Table 1. Comparison of the Mean Sea-Air Flux of Natural CO_2 Estimated From Ocean Inversions[a], Another Forward Model[b], and REF05 (Pg C yr^{-1}) in Different Regions[c]

Region[d]	Latitudes	Ocean inversions[a]	L07[b]	REF05
Polar Southern Ocean	South of 58°S	0.04 ± 0.04	0.25	0.001
South Subpolar Pacific and Indian	44°S–58°S	0.25 ± 0.09	0.27	0.056
South Subpolar Atlantic	44°S–58°S	0.11 ± 0.05	–0.02	–0.004
South Atlantic midlatitude	31°S–44°S	–0.11 ± 0.05	–0.26	–0.076

[a]Fluxes are estimated from an inverse method based on ocean interior observations and transport models with circulation fields from ten ocean general circulation models [*Mikaloff-Fletcher et al.*, 2007]. Shown are the mean and standard deviation of these 10 realizations.
[b]Fluxes simulated by a coarse-resolution coupled ocean-biogeochemical-ecological model [*Lovenduski et al.*, 2007].
[c]Positive values indicate ocean outgassing.
[d]Regions are defined in *Mikaloff-Fletcher et al.* [2007] (see their Figure 2).

[15] The average sea surface temperature (SST) from REF05 is compared to the *Hurrell et al.* [2008] observed climatology in Figure 1 (see also supplementary information). The main differences are found south of 60°S where REF05's SST is too cold, but discrepancies there are difficult to weigh fairly given the scarcity of observations.

[16] Figure 1 compares the average mixed-layer depth (MLD) in winter (July–August–September) for REF05 to the *De Boyer Montégut et al.* [2004] data-based climatology, which was constructed from in situ observations between 1961 and 2008 using a density-difference criterion $\Delta\sigma \leq 0.03$ kg m^{-3}. In the South Pacific and Indian sectors, the observed winter MLD is more localized and deeper than that simulated in REF05. Close to Antarctica, REF05 has shallower winter MLDs, although few data are available in regions with seasonal and permanent sea ice.

[17] The same figure also compares average simulated preindustrial DIC and alkalinity surface concentrations to data-based fields from GLODAP [*Key et al.*, 2004]. For DIC, the largest differences are in the Weddell Sea where simulated values are too low. Generally, simulated DIC is also more annular with more fine-scale features near fronts than found in the GLODAP data product, which is based on sparsely spaced observed cruise tracks. Simulated alkalinity is too low in South Atlantic and Indian sectors (between 30°S and 40°S) and too high in South Pacific (around 60°S). Overall, there is general agreement between simulated and observed DIC and alkalinity, as expected given our relatively short simulations that prevent the model from drifting far away from the initial conditions.

[18] The total of the simulated time-averaged sea-air CO_2 flux integrated spatially over all ocean south of 44°S corresponds to an outgassing of natural carbon of 0.053 Pg C yr^{-1}. Although small, this figure is consistent with the Southern Ocean as a weak source of CO_2 during the preindustrial era (∼0.15 to 0.35 Pg C yr^{-1}) [*Aumont et al.*, 2001; *Mikaloff-Fletcher et al*., 2007; *Gruber et al.*, 2009]. Table 1 compares the average simulated sea-air CO_2 flux to inverse model estimates [*Mikaloff-Fletcher et al.*, 2007] and to that estimated by another forward ocean model [*Lovenduski et al*., 2007]. Including their uncertainties, previous estimates bracket our simulated sea-air CO_2 fluxes in all regions except the South Subpolar Pacific and Indian, where previous estimates are more than twice as large. REF05 produces very weak, near zero outgassing in the Polar Southern Ocean (0.001 Pg C yr^{-1}).

[19] Our simulated results generally agree with both observations and estimates from previous studies. Hence, our modeling framework appears to offer an adequate starting point to understand the response of natural CO_2 flux to positive phases of the SAM. In particular, our decadal simulations are too short for the model to drift significantly from the initial conditions, i.e., from observations. Our approach assesses the sensitivity to the SAM by taking the difference between two simulations, thus largely eliminating drift and systematic bias associated with the mean state.

3.2. Response of CO_2 Fluxes to the SAM

[20] Figure 2 shows maps of the sea-air CO_2 flux for the reference simulation (REF05), the sensitivity simulation ($SAM05^{+++}$), and the anomaly of CO_2 fluxes induced by positive phases of the SAM ($SAM05^{+++}$– REF05). Overall patterns of the total CO_2 fluxes are similar between REF05 and $SAM05^{+++}$, with outgassing at ACC and Antarctic Divergence latitudes as well as along the Chilean coast and Eastern Australia (between 30°S and 50°S) and uptake in the South Atlantic and South Pacific (between 30°S and 40°S) as well as over some sectors close to Antarctica (Antarctic Peninsula, South Pacific sector, and north of the Cooperation Sea). But positive SAM events generally intensify outgassing (or reduce uptake) of natural CO_2 south of the STF, especially north of the Weddell Sea, the Cooperation Sea, and the Ross Sea. Conversely, there is generally intensified uptake (or less outgassing) of natural CO_2 north of the STF. Adjacent to Antarctica, positive SAM events lead to small changes in fluxes but a complex spatial distribution. Fluxes are small in terms of the annual mean (Figure 2), but in regions adjacent to Antarctica, they can be large in months when sea ice is absent. Although the spatial pattern of the response of the sea-air CO_2 flux to the SAM is roughly annular, our eddy-permitting model exhibits greater spatial variability than do coarse-resolution models [e.g., *Lovenduski et al.*, 2007; *Lenton and Matear*, 2007], partly because its frontal structures are less zonal.

[21] Figure 3 shows mean CO_2 fluxes computed from REF05 simulation and anomalies of CO_2 fluxes induced by a SAM perturbation of one standard deviation in the different interfrontal regions as well as the total, integrated across the entire Southern Ocean. In the three southernmost regions (AZ, PFZ, SAZ), mean fluxes of natural CO_2 are from the ocean to the atmosphere, while in the STZ, the flux is from the atmosphere to the ocean. When integrated over the entire Southern Ocean (south of 31°S), the response of the CO_2 flux to one standard deviation of the SAM is 0.1 Pg C yr^{-1}, similar to that found by *Lovenduski et al.* [2007] and *Lenton and Matear* [2007]. During positive phases of the SAM,

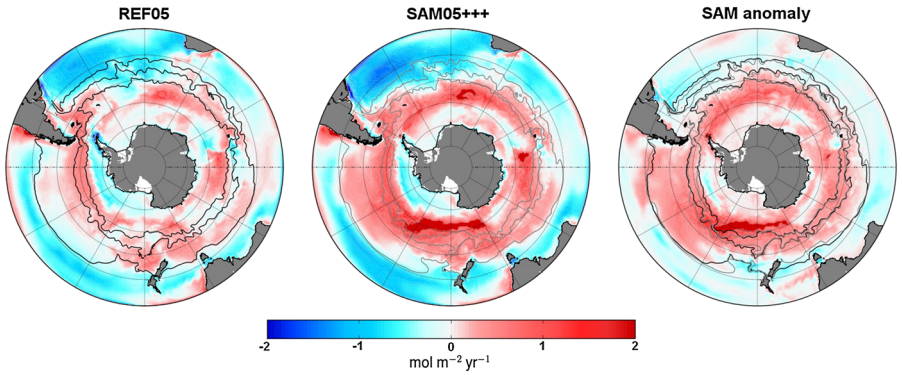

Figure 2. Mean (1995–2004) sea-air CO_2 fluxes in (left) REF05, (middle) SAM05^{+++}, and (right) the SAM05^{+++}–REF05 anomaly in mol m^{-2} yr^{-1}. Contours correspond to mean positions of fronts in (black) REF05 and (gray) SAM05^{+++}. Positive fluxes indicate ocean outgassing. (Right) Note the large positive anomalies (intensified outgassing) in the Antarctic Divergence north of the Weddell Sea, the Cooperation Sea, and the Ross Sea.

there is enhanced outgassing in the AZ, PFZ, and SAZ but enhanced uptake in STZ, consistent with Figure 2. The AZ dominates the Southern Ocean response of natural CO_2 fluxes to the SAM, showing an anomaly more than 2.5 times greater than in any other regions.

3.3. Component Analysis

[22] To investigate causes of the response of CO_2 fluxes to positive phases of the SAM, we carried out a component analysis [*Takahashi et al.*, 1993], computing the total derivative of CO_2 fluxes with respect to positive phases of the SAM. From equation (1), CO_2 fluxes depend on k, α, f_{ice}, and pCO_2^{oc}, since pCO_2^{atm} is constant in our simulations. The CO_2 fluxes can be thus partitioned into the following contributions:

$$\Delta F_{calcul} = \frac{\partial F}{\partial k}\Delta k + \frac{\partial F}{\partial \alpha}\Delta \alpha + \frac{\partial F}{\partial f_{ice}}\Delta f_{ice} + \frac{\partial F}{\partial pCO_2^{oc}}\Delta pCO_2^{oc} \quad (2)$$

where F is the sea-air CO_2 flux and Δ indicates the anomaly computed from the difference between SAM05^{+++} and REF05 simulations. The different terms are computed from 5 day output averaged over 1995–2004. In each region, most of the response of CO_2 fluxes to the SAM is due to the change in pCO_2^{oc}, which drives 68% of the response on average, while k (wind speed variation) largely explains the remaining response. Contributions from solubility and sea ice fraction are less than 2% and are thus neglected in subsequent analyses.

[23] Changes in the dominant factor, pCO_2^{oc}, can be decomposed further into contributions from surface DIC, alkalinity (Alk), temperature (SST), and salinity (SSS). Since variations in SST and SSS have a small effect on k, we only consider the effect of wind velocity (W). Hence, the total derivative of sea-air CO_2 fluxes can be further decomposed into the following contributions:

$$\Delta F_{calcul} = \frac{\partial F}{\partial W}\Delta W + \frac{\partial F}{\partial DIC}\Delta DIC + \frac{\partial F}{\partial Alk}\Delta Alk + \frac{\partial F}{\partial SST}\Delta SST + \frac{\partial F}{\partial SSS}\Delta SSS \quad (3)$$

[24] Partial derivatives are computed following *Sarmiento and Gruber* [2006, p. 332–339].

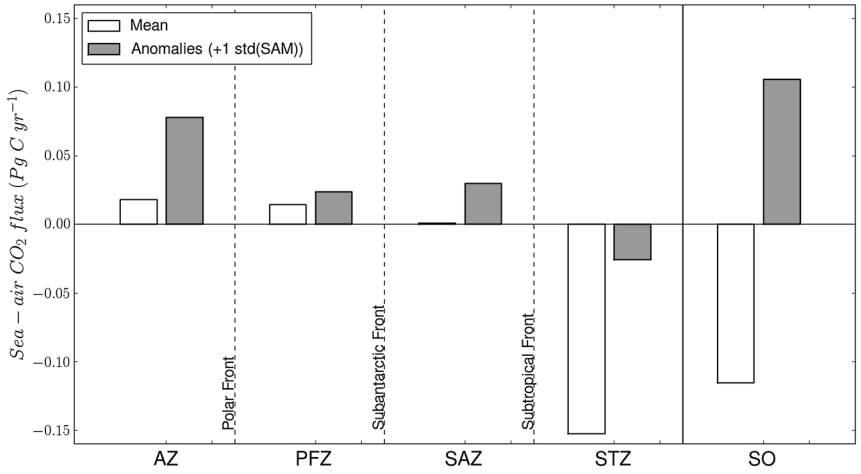

Figure 3. Mean (1995–2004) sea-air CO_2 flux (white) from REF05 simulation and (gray) from the response to +1 standard deviation of the SAM in Pg C yr^{-1} integrated over the different interfrontal regions and over the entire Southern Ocean (SO).

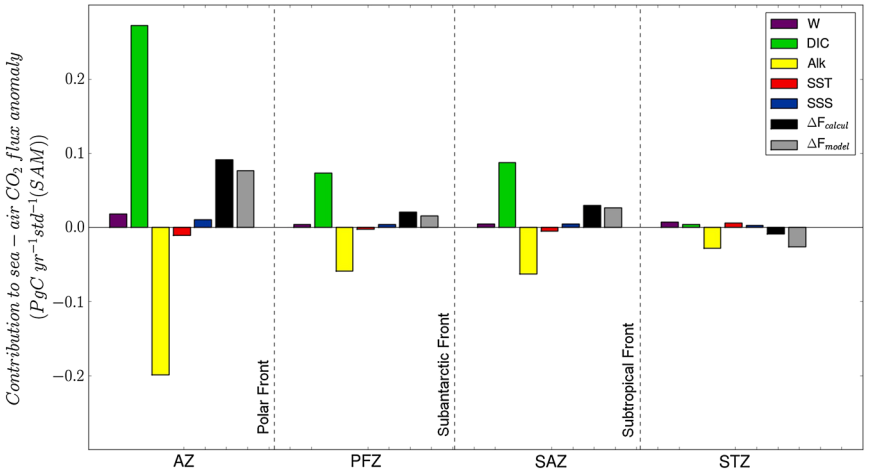

Figure 4. Contributions to sea-air CO_2 flux response to the SAM from components described in equation (3), in Pg C yr^{-1} std^{-1}(SAM) and integrated into the different interfrontal regions. $\Delta F_{\mathrm{calcul}}$ is the sum of all contributions while $\Delta F_{\mathrm{model}}$ is the simulated sea-air CO_2 flux response to the SAM. Note that the gray bars of $\Delta F_{\mathrm{model}}$ are the same as in Figure 3.

[25] Figure 4 shows the results of the component analysis described in equation (3) for the four regions. Contributions of the different components, in Pg C yr^{-1} std^{-1}(SAM), are shown accounting for the total area of each interfrontal region. There are residual differences between $\Delta F_{\mathrm{model}}$, the term directly computed from the difference between the two simulations, and $\Delta F_{\mathrm{calcul}}$ that computed as the sum of the contributions in equation (3). Those differences are generally small except in the STZ. The discrepancy may result from the underlying assumption that changes occur only as small linear perturbations relative to the mean state. Moreover, approximations in the calculation of contributions and cross-correlations among the variables may also explain the discrepancy.

[26] Figure 4 shows that the AZ dominates the response of sea-air CO_2 fluxes to the SAM because it has both the strongest fluxes and the largest surface area. In the AZ, changes in DIC, SSS, and W enhance CO_2 outgassing (or reduce uptake) while changes in Alk and SST reduce CO_2 outgassing (or enhance uptake). In all regions, positive phases of the SAM enhance both DIC and alkalinity, which are the main drivers of changes, except in the STZ where alkalinity alone dominates. The SSS increase and SST decrease drive only modest changes in positive SAM-induced sea-air CO_2 flux. Contribution of wind velocity is strongest in the AZ but remains small in all regions.

[27] As a check on the component analysis approach, we repeated the analysis following the approach of *Lovenduski et al.* [2007], where DIC and alkalinity are salinity normalized (not shown). While salinity-normalized DIC and alkalinity show dominant contributions to the response of CO_2 flux to the SAM, freshwater fluxes (responsible for diluting or concentrating surface DIC and alkalinity) show a similar contribution as SSS. Thus, SSS-driven changes in the CO_2 flux with positive phases of the SAM are mainly caused by changes in freshwater fluxes, probably from enhanced evaporation driven by stronger westerlies or from changes in surface salinity restoring. Conversely, changes in DIC and alkalinity are not driven by freshwater fluxes but rather interior ocean processes such as biogeochemical processes or advection and diffusion. These will be distinguished below.

3.4. Causes of DIC Changes in the Mixed Layer of the Antarctic Zone

[28] Here we separate and quantify the main terms that cause mixed-layer DIC to change, computing a term balance following the approach of *Vialard and Delecluse* [1998] for temperature and salinity. The tendency in DIC is deconvolved into the contributions from each process that is represented in the model. The depth-averaged DIC concentration in the mixed-layer ($\mathrm{DIC_{ML}}$) varies as,

$$\partial_t \mathrm{DIC_{ML}} = \underbrace{-\frac{1}{H}\int_{-H}^{0} \vec{U}\cdot\vec{\nabla}\mathrm{DIC}\,\mathrm{d}z}_{\text{advection}} \underbrace{-\frac{1}{H}\left(\mathrm{DIC_{ML}}-\mathrm{DIC}_{-H}\right)\partial_t H}_{\text{entrainment/detrainment}} \underbrace{-\frac{1}{H}\int_{-H}^{0} D_l(\mathrm{DIC})\,\mathrm{d}z-\frac{1}{H}\left[\kappa_z\partial_z\mathrm{DIC}\right]_{-H}}_{\text{diffusion}} + \underbrace{fw}_{\text{dilution/concentration}} + \underbrace{bio}_{\text{biology}} + \underbrace{flx}_{\text{sea–air fluxes}} \quad (4)$$

where H is the time-varying depth of the mixed layer (ML), $\vec{U}$ is the velocity field, D_l is the effective model isoneutral diffusion operator of DIC, κ_z is the vertical diffusion coefficient, *fw* accounts for dilution and concentration effects on DIC concentration, *bio* represents "biological" processes that include organic matter production, remineralization, and the carbonate cycle, and *flx* is the sea-air CO_2 flux. The velocity $\vec{U}$ can be further decomposed into zonal, meridional, and vertical advection of DIC in the mixed layer. In our eddy-permitting model, unresolved advection is represented by a subgrid scale closure scheme of diffusion and is decomposed into diffusion along isoneutral surfaces (left-hand term) and vertical diffusion at the base of mixed layer (right-hand term). Eddies thus contribute to this DIC budget both via advection (resolved part) and isoneutral diffusion (unresolved part); conversely, in a coarse-resolution

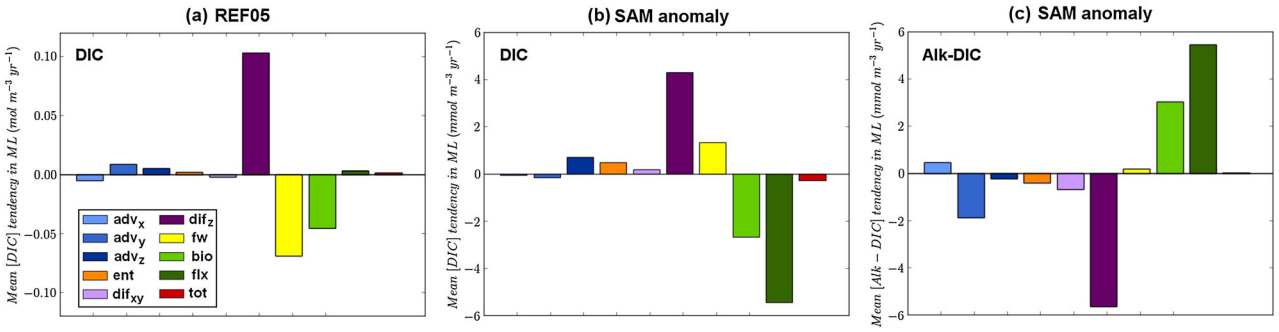

Figure 5. Mixed-layer 1995–2004 time-averaged tendencies of (a, b) DIC and (c) Alk-DIC for each process integrated over the AZ for REF05 (Figure 5a) and the SAM anomaly (Figures 5b and 5c) (SAM05^{+++}–REF05). The adv_x, adv_y, and adv_z are, respectively, the zonal, meridional, and vertical advection tendency terms, *ent* is the entrainment tendency term, dif_{xy} and dif_z are, respectively, the isoneutral and vertical diffusion tendency terms, *fw* is the dilution-concentration tendency term, *bio* is the biological tendency term, *flx* is the sea-air CO_2 flux tendency term following equation (4), and *tot* is the total tendency term. Positive values indicate a gain of DIC (Figures 5a and 5b) and Alk-DIC (Figure 5c) concentration. Note that scales are different between Figure 5a and Figures 5b and 5c.

model with an eddy-transport parameterization [e.g., *Gent and McWilliams*, 1990], eddies would only contribute via isoneutral diffusion. In the model, the DIC term balance is computed online, with tendency terms from each time step summed over a 5 day time window and the total tendency term calculated as the difference between final and initial states over the 5 day time window. The entrainment term is thus computed as a residual term over each 5 day time window, limited only by numerical precision of the computer (12 significant figures). This analysis is performed for REF05 and SAM05^{+++} simulations during the period 1995–2004.

[29] Figures 5a and 5b show the 5 day time-averaged DIC tendencies for each process integrated in the AZ and averaged over 1995–2004 for the REF05 simulation and the SAM anomaly (SAM05^{+++}–REF05).

3.4.1. DIC Mean State

[30] Both the REF05 and SAM05^{+++} simulations have generally similar tendencies for the different terms (Figure 5a for REF05). Vertical diffusion is the main process that acts to increase mixed-layer DIC, while biology and dilution reduce it. Contributions from advection, isoneutral diffusion, entrainment, and sea-air fluxes are small. Processes are similarly partitioned in all the other interfrontal zones (see supporting information).

[31] The intensity of vertical diffusion of DIC at the base of the mixed layer depends upon vertical gradients of DIC. Mean vertical profiles and vertical gradients of DIC in the AZ are shown in Figure 6a. There are strong vertical gradients of DIC across the base of the mixed layer, which explains the associated intense vertical diffusion of DIC. In the mixed layer, the stratification in DIC concentration is

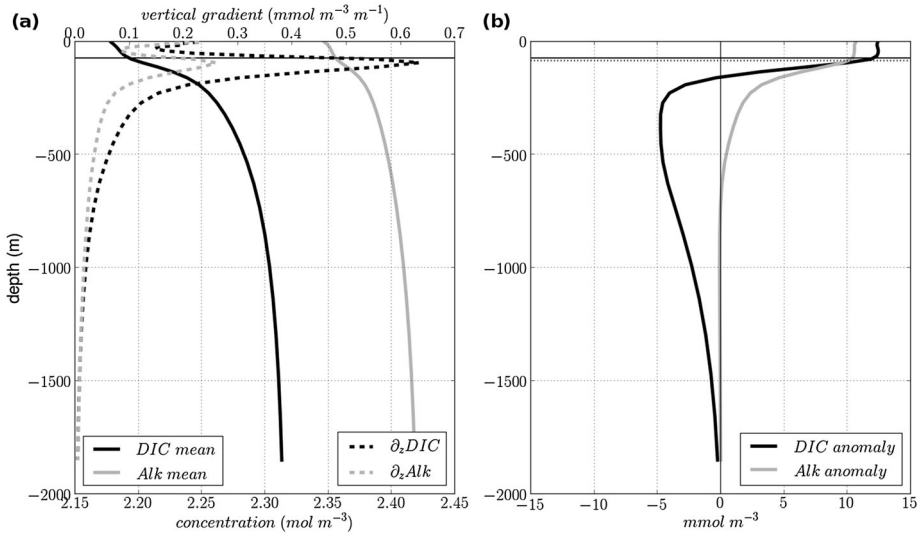

Figure 6. (a) The mean AZ vertical profiles (solid lines) and vertical gradients (dashed lines) of DIC and alkalinity over 1995–2004 for the REF05 simulation. (b) The vertical profile anomalies to positive phases of the SAM. The horizontal black line indicates the AZ-averaged mixed-layer depth in REF05 (Figures 6a and 6b), while the dotted line is for SAM05^{+++} (Figure 6b).

weaker but well-maintained, probably because surface DIC is consumed by biological processes and reduced by CO_2 outgassing.

3.4.2. Response of DIC in the Mixed Layer

[32] The SAM-induced anomalies in the tendency terms differ from the mean state in how the processes are partitioned (Figure 5b). Vertical diffusion is the main process that acts to increase DIC in the mixed layer during positive phases of the SAM, while both biology and the sea-air CO_2 flux tend to compensate for this increase. In response to the SAM, dilution is reduced while contributions from advection, entrainment, and isoneutral diffusion only experience small changes. Although it increases slightly in response to positive phases of the SAM, vertical advection does not contribute much to the increase in DIC in the AZ's mixed layer nor in other interfrontal zones (see supporting information).

[33] In response to the SAM, the AZ's mixed layer deepens by 13 m on average (Figure 6b) mostly in the Antarctic Divergence (see supporting information), thus reaching a steeper local vertical gradient of DIC (Figure 6a). This enhances vertical diffusion of DIC at the base of the mixed layer. The contribution of biology may result from the enhanced mixed-layer depth, that is if the resulting increase in nutrient availability is not outcompeted by stronger light limitation. The contribution of the sea-air flux merely corresponds to the intense outgassing of CO_2 at the Antarctic Divergence, thus decreasing DIC in the mixed layer. The decrease of dilution under positive phases of the SAM is likely to result from the reduction in freshwater input to the ocean as sea ice melting is lower. Moreover, with positive SAM, the mixed layer is deeper, thus reducing the impact of surface freshwater flux changes over the mixed-layer DIC. Entrainment is expected to have little influence on the mean state of DIC in the mixed layer, because its effect is found to essentially cancel over the full seasonal cycle (see Figure 5a). Hence, it makes a negligible contribution to the SAM-driven change in mixed-layer DIC, estimated from the difference between two mean states (i.e., $SAM05^{+++}$–REF05).

[34] Although large-scale vertical advection (i.e., upwelling) is crucial to supply DIC and support its vertical gradient below the mixed layer, this is not the dominant means by which DIC effectively enters into the mixed layer. Rather, the main mechanism is through turbulent fluxes at the base of the mixed layer, which are represented by vertical diffusion in our model. Hence, the paradigm where the SAM-induced outgassing of natural CO_2 is mainly driven by enhanced wind-driven upwelling that in turn directly brings more DIC to the surface [*Lovenduski et al.*, 2007; *Lenton and Matear*, 2007] requires modification. The same two previous studies also suggest that biology plays a negligible role in driving DIC changes in response to the SAM. Conversely, we find that in the AZ, the biologically driven response is substantial although somewhat less than the response due to vertical diffusion.

3.5. Partial Alkalinity Compensation

[35] In our model, the response of natural CO_2 flux to the SAM is mainly driven by enhancements of DIC and alkalinity whose effects oppose one another. Equal increases in surface DIC and alkalinity lead to nearly no change in pCO_2^{oc}, which drives the sea-air CO_2 flux, as illustrated by a plot of pCO_2^{oc} as a function of these two conservative tracers (supporting information). The reason is that alkalinity minus DIC is roughly equal to carbonate ion concentration [*Broecker and Peng*, 1982; *Sarmiento and Gruber*, 2006], which if constant induces no change in pCO_2^{oc}. Positive SAM events enhance both DIC and alkalinity directly below the AZ's mixed layer (Figure 6b). The associated anomaly in the Alk-DIC difference is negative in the mixed layer, while positive just below it.

[36] The causes of these differences are revealed by the tendency terms for the physical and biological processes in the AZ's mixed layer (Figure 5c). The mixed-layer surplus of DIC relative to alkalinity cannot be explained by gas exchange, the only process affecting the former but not the latter, because outgassing reduces DIC, nor can it be explained by biology as that decreases DIC while increasing alkalinity (more positive Alk-DIC). Rather, the main process acting to increase DIC more than alkalinity (negative Alk-DIC) in the AZ's mixed layer is enhanced vertical diffusion during positive SAM events. The intensity of vertical diffusion differs for DIC and alkalinity because they have different vertical tracer gradients across the base of the mixed layer. Mean vertical gradients of DIC in the AZ are stronger than those of alkalinity directly below the mixed layer (Figure 6a). Thus, deepening of the mixed layer in response to positive SAM events reaches steeper vertical gradients of DIC relative to those for alkalinity, thereby favoring upward diffusion of the former over the latter.

3.6. Eddy Compensation in Ocean Interior

[37] When the mixed layer deepens, strong vertical gradients of DIC drive enhanced vertical diffusion of DIC at the base of the mixed layer. Thus, we analyzed a major determinant of the subsurface DIC supply at the Antartic Divergence, namely the balance of meridional fluxes of DIC. Meridional transport of DIC is computed as a function of potential density in the same way that many previous studies have computed volume transport [e.g., *Hallberg and Gnanadesikan*, 2006; *Farneti et al.*, 2010]. Potential density is used rather than depth to better represent transport of water masses [e.g., *Treguier et al.*, 2007]. Yet unlike volume transport, DIC transport cannot be described precisely by a stream function, because $\vec{U} \times \mathrm{DIC}$ is divergent whereas $\vec{U}$ is not. Strictly speaking, one cannot follow streamlines of the zonally averaged meridional DIC flux, but it is accurate to study the associated intensity and direction of the flux at a given latitude and density. To compute the total meridional flux of DIC, its transport is averaged zonally along constant potential density surfaces and then integrated vertically:

$$\Gamma_{tot}(y,\sigma_2) = \overline{\oint \int_{-H}^{\tilde{z}(x,y,\sigma_2)} v \cdot \mathrm{DIC}\, d\tilde{z}'\, dx} \tag{5}$$

where σ_2 is the 2000 m reference potential density, H is the spatially varying bottom depth, and $\tilde{z}$ is the depth of the σ_2 isopycnal. The overbar denotes the time average over 1995–2004, while v is the 5 day-averaged meridional velocity and DIC refers to its concentration. To quantify how eddies affect the DIC response to the SAM, the total meridional flux of DIC is decomposed into three contributions following the approach for water transport [*Dufour et al.*, 2012]:

$$\Gamma_{\mathrm{tot}} = \Gamma_{\mathrm{zon}} + \Gamma_{\mathrm{SE}} + \Gamma_{\mathrm{TE}} \tag{6}$$

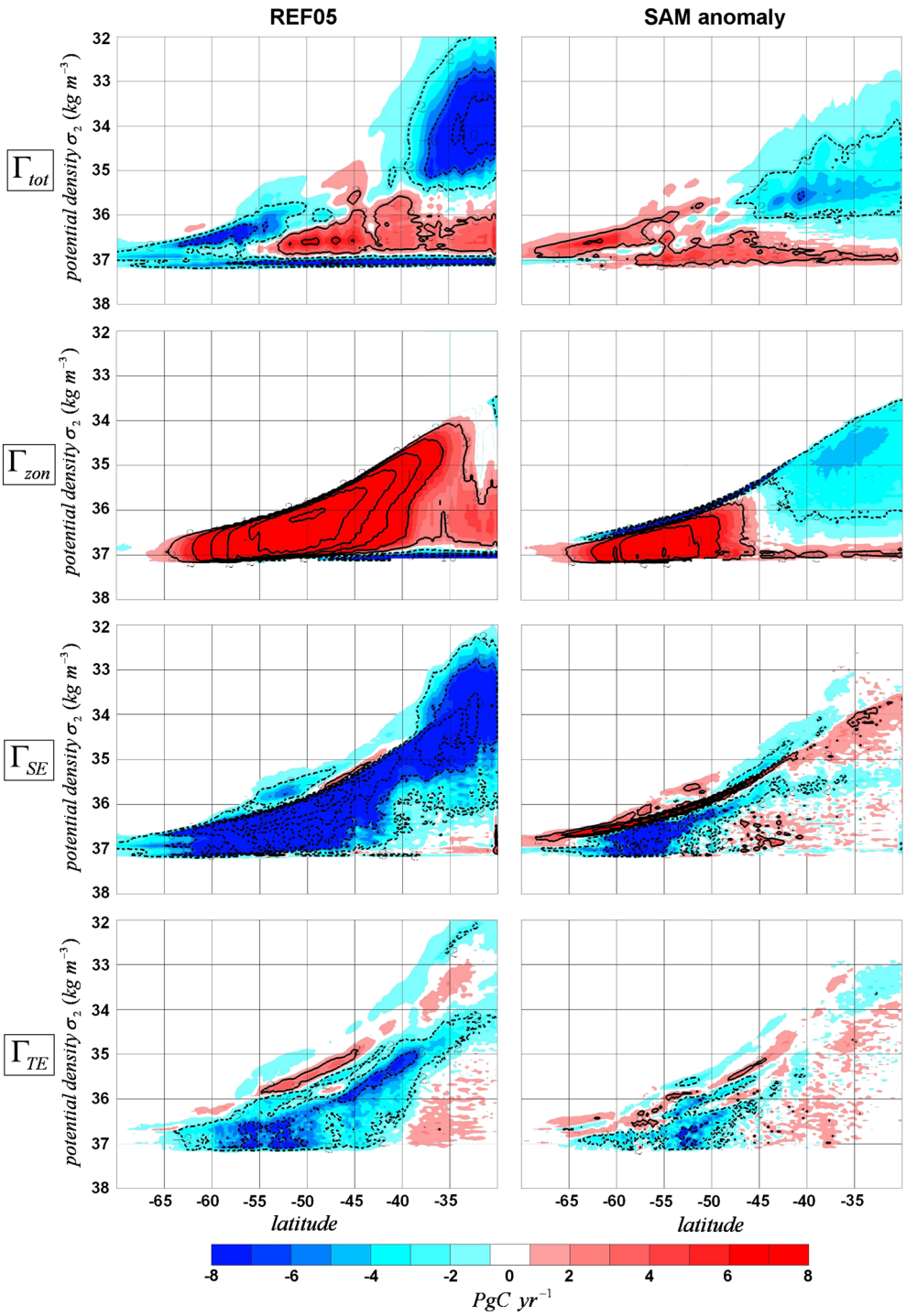

Figure 7. (Top) Total transport of DIC by density class in Pg C yr^{-1} and separated into its three contributions (see section 3.6) for (left) REF05 and (right) the SAM anomaly ($SAM05^{+++}$–REF05). Red cells are clockwise and blue cells are counterclockwise.

The first component Γ_{zon} is the transport by the zonal mean flow, which is associated with the northward Ekman transport in shallow layers and the southward geostrophic transport in layers below the sill depth of Drake Passage. The second component Γ_{SE} is the transport by standing eddies, defined as meridional deviations from a zonal mean. Standing eddy transport includes that from stationary meanders as well as the large-scale meanders of the ACC. The third component Γ_{TE} is the transport from transient eddies, defined as deviations from the time mean following *Treguier et al.* [2007]. Transient eddy transport is that associated with time-varying features of ocean circulation (e.g., frontal waves, rings, eddies, and meanders).

[38] Figure 7 shows the result of this decomposition for both the reference simulation (REF05) and the anomaly ($SAM05^{+++}$–REF05). In REF05, the total DIC flux (Γ_{tot})

displays a clockwise cell which extends up to ~55°S and is called the *subpolar cell*. The subpolar cell corresponds to a circulation where DIC-rich NADW from the north are brought to the surface near the Antarctic Divergence by Ekman pumping, are transformed into AAIW by surface fluxes, and are returned north as intermediate waters. Here we thus focus on the subpolar cell because it is the cell-controlling DIC supply to the subsurface at the Antarctic Divergence.

[39] In REF05, the total DIC flux brought to the subsurface of the Antarctic Divergence reaches ~7 Pg C yr^{-1}. This total flux is mainly driven by the vigorous wind-driven DIC flux (Γ_{zon}) that reaches ~22 Pg C yr^{-1} and is centered at latitudes of the ACC. This wind-driven flux component comes up near the subsurface of the Antarctic Divergence and flows back northward, driven by Ekman pumping and Ekman transport in the Ekman layer. The two other components partially compensate the wind-driven DIC flux: The standing eddy-induced DIC flux (Γ_{SE}) reaches its ~22 Pg C yr^{-1} maximum in shallow layers between 45°S and 60°S, while the transient eddy-induced DIC flux (Γ_{TE}) reaches its ~10 Pg C yr^{-1} maximum in deeper layers between 40°S and 60°S. The compensation by the standing eddy component is likely from small-scale meanders rather than large-scale meanders or even basin-scale gyres [*Ballarotta et al.*, 2013].

[40] Positive SAM events intensify the total meridional DIC flux by ~2 Pg C yr^{-1}, the final balance of the three stronger components. Simultaneously, there is a poleward shift of the subpolar cell by ~2°–3°, corresponding to the poleward shift in the westerlies. A simple metric of the change in subpolar cell intensity is to average its DIC transport between 40°S and 60°S. With that, the anomaly in the total DIC flux increases by ~6% std^{-1}(SAM), with more brought to the subsurface near the Antarctic Divergence. The main driver is the wind-driven DIC flux that is intensified by ~10% std^{-1}(SAM), but that is partly compensated by the total eddy-induced DIC flux: the standing eddy component intensifies by ~4% std^{-1}(SAM) while the transient eddy component strengthens by ~15% std^{-1}(SAM). Overall, our intermediate-resolution model study suggests that about one third of the SAM-induced increase in wind-driven northward DIC flux is compensated by transport associated with standing and transient eddies.

4. Discussion

[41] Our study with a regional 0.5° eddying model of the Southern Ocean reveals substantial differences between a reference simulation and a perturbation where winds were permanently shifted poleward and intensified following the observed pattern of the SAM. That SAM perturbation enhances outgassing of natural CO_2 mainly because surface DIC increases, even though its effect is compensated by enhanced surface alkalinity; conversely, previous studies emphasized the dominant role of changes in winds and SST [*Lovenduski et al.*, 2007; *Lenton and Matear*, 2007]. In the AZ, the DIC increase in response to the SAM occurs mainly because of enhanced vertical diffusion at the base of the mixed layer, a process that previous studies did not investigate. That enhancement came not from enhanced κ_z but from the SAM driving the base of the mixed layer deeper, where vertical gradients in DIC are steeper, being maintained by large-scale upwelling of deeper waters rich in DIC. Large-scale upwelling is also affected by the SAM, with associated eddy-driven DIC transport compensating about one third of the enhanced Ekman-driven DIC transport.

[42] Differences in our experimental design may partially explain discrepancies with previous studies in terms of the effects related to alkalinity versus those from SST and winds. First, our simulations did not account for covariations with atmospheric variables, such as air temperature [*Sen Gupta and England*, 2006]. Thus, they may underestimate how SST influences the response of the sea-air CO_2 flux to positive SAM events. Second, our permanent perturbation offers a means to address the long-term response to the positive trend in the SAM, but it does not address changes associated with the SAM's high-frequency variability. In particular, on time scales of a few months, positive SAM events cool the surface ocean and increase northward Ekman transport. But on long time scales of years to few decades, the circulation tends to adjust to a new equilibrium, altering vertical profiles of DIC and alkalinity. Previous studies that regress variables onto the SAM index have emphasized the transient response to SAM events, for which winds and SST are major drivers [*Lovenduski et al.*, 2007; *Lenton and Matear*, 2007]. More recent studies based on computing long-term trends by variable [*Lovenduski et al.*, 2008] or comparing mean states between two simulations (this study) emphasize the long-term response to the increased positive trend in SAM events. They provide a means to assess the effect of large-scale modifications in circulation, which modify DIC and alkalinity vertical profiles and thus the sea-air CO_2 flux.

[43] The importance of vertical gradients of DIC across the base of the mixed layer in constraining the response of sea-air CO_2 fluxes to changes in winds was acknowledged by *Mahadevan et al.* [2011], though not in the context of the SAM. As long as the vertical gradient of DIC below the mixed layer is positive and steeper than that at its base (after correction for alkalinity compensation), positive SAM events will enhance the sea-air CO_2 flux, because they deepen the mixed layer. Thus, the immediate response is CO_2 outgassing, because the mixed layer deepens before subsurface vertical gradients of DIC and alkalinity have a chance to be modified due to deeper, longer-term changes in transport or mixed-layer processes. Hence, it is the change in vertical gradient of DIC minus alkalinity at and below the mixed-layer depth that determines the long-term response of the sea-air CO_2 flux to the SAM.

[44] Across the base of the mixed layer, vertical gradients of DIC are mainly determined by a combination of loss by vertical diffusion into the mixed layer and supply by the upward and poleward transport below the mixed layer. Our simulations demonstrate that about one third of the wind-driven enhancement of upward and poleward transport of DIC is compensated by eddy transport, suggesting that coarse models may overestimate the response of CO_2 fluxes to the SAM. Since our model only partially resolves the eddy spectrum, this eddy compensation may increase with increasing resolution. Yet full eddy compensation may be unachievable, because Ekman and eddy fluxes act at different depths [*Morrison and Hogg*, 2013]. Our study provides a first step toward quantifying the potential role of mesoscale

eddies in the response of the Southern Ocean natural CO_2 flux to the SAM, and its results confirm the need for similar studies at higher resolution.

[45] **Acknowledgments.** C.O. Dufour was supported by the French CEA (Commissariat à l'Energie Atomique et aux Energies Alternatives). Funding for this study came from the European Project on Ocean Acidification (EPOCA) funded by the European Community's Seventh Framework Programme (FP7/2007-2013) under grant agreement 211384, as well as by the EU FP7 project CarboChange (grant agreement 264879). J. Le Sommer and B. Barnier were supported by the French CNRS (Centre National de la Recherche Scientifique). This work benefited from funding of the ANR (through contract ANR-08-JCJC-0777-01) and from CNRS through LEFE/INSU program (project CO2SUD). This work was granted access to the HPC resources of [CCRT/TGCC/CINES/IDRIS] under the allocation 2011-016035 made by GENCI (Grand Equipement National de Calcul Intensif). Simulations were carried out at the CINES super computer facility in Montpellier, France. We thank C. Ethé, L. Bopp, and O. Aumont for providing initialization fields and for discussions about model setup, analysis, and results. We also thank L. Merlivat for her advice on the mixed-layer term balance analysis.

References

Aumont, O., and L. Bopp (2006), Globalizing results from ocean in situ iron fertilization studies, *Global Biogeochem. Cycles*, *20*, GB2017, doi:10.1029/2005GB002591.

Aumont, O., J. C. Orr, P. Monfray, W. Ludwig, P. Amiotte-Suchet, and J.-L. Probst (2001), Riverine-driven interhemispheric transport of carbon, *Global Biogeochem. Cycles*, *15*, 393–405.

Ballarotta, M., S. Drijfhout, T. Kuhlbrodt, and K. Döös (2013), The residual circulation of the Southern Ocean: Which spatio-temporal scales are needed?, *Ocean Modell.*, *64*, 46–55.

Barnola, J.-M., D. Raynaud, Y. Korotkevich, and C. Lorius (1987), Vostok ice core provides 160,000-year record of atmospheric CO_2, *Nature*, *329*, 408–418.

Böning, C., A. Dispert, M. Visbeck, S. Rintoul, and F. Schwarzkopf (2008), The response of the Antarctic Circumpolar Current to recent climate change, *Nat. Geosci.*, *1*, 864–869.

Brodeau, L., B. Barnier, T. Penduff, A.-M. Treguier, S. Gulev, and T. J. McDougall (2010), An ERA-40 based atmospheric forcing for global ocean circulation models, *Ocean Modell.*, *31*, 88–104.

Broecker, W. S., and T. H. Peng (1982), *Tracers in the Sea*, Lamont-Doherty Geological Observatory, Palisades, N. Y.

Conkright, M. E., R. A. Locarnini, H. E. Garcia, T. D. O'Brien, T. P. Boyer, C. Stephens, and J. I. Antonov (2002), World ocean database 2001: Objective analyses, data statistics and figures.

Cunningham, S. A., S. G. Alderson, B. A. King, and M. A. Brandon (2003), Transport and variability of the Antarctic Circumpolar Current in Drake Passage, *J. Geophys. Res.*, *108*(C5), 8084, doi:10.1029/2001JC001147.

De Boyer Montégut, C., G. Madec, A. S. Fischer, A. Lazar, and D. Iudicone (2004), Mixed layer depth over the global ocean: An examination of profile data and a profile-based climatology, *J. Geophys. Res.*, *109*, C12003, doi:10.1029/2004JC002378.

Drakkar Group (2007), Eddy-permitting ocean circulation hindcasts of past decades, *CLIVAR Exch.*, *12*, 8–10.

Dufour, C. O., J. Le Sommer, T. Penduff, B. Barnier, and M. H. England (2011), Structure and causes of the pulsation mode in the Antarctic Circumpolar Current south of Australia, *J. Phys. Oceanogr.*, *41*, 253–268.

Dufour, C. O., J. Le Sommer, J. D. Zika, M. Gehlen, J. C. Orr, P. Mathiot, and B. Barnier (2012), Standing and transient eddies in the response of the Southern Ocean meridional overturning to the southern annular mode, *J. Clim.*, *25*, 6958–6974.

Farneti, R., T. L. Delworth, A. J. Rosati, S. M. Griffies, and F. Zeng (2010), The role of mesoscale eddies in the rectification of the Southern Ocean response to climate change, *J. Phys. Oceanogr.*, *40*, 1539–1557.

Fichefet, T., and M. A. M. Maqueda (1997), Sensitivity of a global sea ice model to the treatment of ice thermodynamics and dynamics, *J. Geophys. Res.*, *102*, 12,609–12,646.

Gent, P. R., and J. C. McWilliams (1990), Isopycnal mixing in ocean circulation models, *J. Phys. Oceanogr.*, *20*, 150–155.

Gouretski, V., and K. Koltermann, (2004), WOCE Global Hydrographic Climatology, a technical report, *Berichte des BSH, 35.*

Griffies, S. M., et al. (2009), Coordinated Ocean-ice Reference Experiments (COREs), *Ocean Modell.*, *26*, 1–46.

Gruber, N., et al. (2009), Oceanic sources, sinks and transport of atmospheric CO_2, *Global Biogeochem. Cycles*, *23*, GB1005, doi:10.1029/2008GB003349.

Hallberg, R., and A. Gnanadesikan (2006), The Role of Eddies in Determining the Structure and Response of the Wind-Driven Southern Hemisphere Overturning: Results from the Modeling Eddies in the Southern Ocean (MESO) Project, *J. Phys. Oceanogr.*, *36*, 2232–2252.

Hurrell, J. W., J. J. Hack, D. Shea, J. M. Caron, and J. Rosinski (2008), A new sea surface temperature and sea ice boundary dataset for the community atmosphere model, *J. Clim.*, *21*, 5145–5153.

Key, R. M., A. Kozyr, C. L. Sabine, K. Lee, R. Wanninkhof, J. L. Bullister, R. A. Feely, F. J. Millero, C. Mordy, and T.-H. Peng (2004), A global ocean carbon climatology: Results from Global Data Analysis Project (GLODAP), *Global Biogeochem. Cycles*, *18*, GB4031, doi:10.1029/2004GB002247.

Lachkar, Z., J. Orr, J.-C. Dutay, and P. Delecluse (2007), Effects of mesoscale eddies on global ocean distributions of CFC-11, CO_2 and $\delta^{14}C$, *Ocean Sci.*, *3*, 461–482.

Lachkar, Z., J. C. Orr, and J.-C. Dutay (2009a), Seasonal and mesoscale variability of oceanic transport of anthropogenic CO_2, *Biogeosciences*, *6*, 2509–2523.

Lachkar, Z., J. C. Orr, J.-C. Dutay, and P. Delecluse (2009b), On the role of mesoscale eddies in the ventilation of Antarctic intermediate water, *Deep Sea Res. I*, *56*, 909–925.

Le Quéré, C., et al. (2007), Saturation of the Southern Ocean CO_2 Sink due to recent climate change, *Science*, *316*, 1735–1738.

Le Quéré, C., T. Takahashi, E. T. Buitenhuis, C. Rödenbeck, and S. C. Sutherland (2010), Impact of climate change and variability on the global oceanic sink of CO_2, *Global Biogeochem. Cycles*, *24*, GB4007, doi:10.1029/2009GB003599.

Lenton, A., and R. J. Matear (2007), Role of the southern annular mode (SAM) in Southern Ocean CO_2 uptake, *Global Biogeochem. Cycles*, *21*, GB2016, doi:10.1029/2006GB002714.

Lenton, A., F. Codron, L. Bopp, N. Metzl, P. Cadule, A. Tagliabue, and J. Le Sommer (2009), Stratospheric ozone depletion reduces ocean carbon uptake and enhances acidification, *Geophys. Res. Lett.*, *36*, L12606, doi:10.1029/2009GL038227.

Levitus, S., T. Boyer, M. Conkright, T. O'Brien, J. Antonov, C. Stephens, L. Stathoplos, D. Johnson, and R. Gelfeld (1998), *World Ocean Database 1998, NOAA Atlas NESDID 18*, 150, vol. 40, US Governement Printing Office, Washington, D. C.

Lovenduski, N., N. Gruber, S. Doney, and I. Lima (2007), Enhanced CO_2 outgassing in the Southern Ocean from a positive phase of the Southern Annular Mode, *Global Biogeochem. Cycles*, *21*, GB2026, doi:10.1029/2006GB002900.

Lovenduski, N., N. Gruber, and S. Doney (2008), Toward a mechanistic understanding of the decadal trends in the Southern Ocean carbon sink, *Global Biogeochem. Cycles*, *22*, GB3016, doi:10.1029/2007GB003139.

Lovenduski, N., M. Long, P. Gent, and K. Lindsay (2013), Multi-decadal trends in the advection and mixing of natural carbon in the Southern Ocean, *Geophys. Res. Lett.*, *40*, 139–142, doi:10.1029/2012GL054483.

Madec, G. (2008), Nemo ocean engine, *Note du Pôle de modelisation, Institut Pierre-Simon Laplace (IPSL), France, 27*, ISSN 1288–1619.

Madec, G., P. Delecluse, M. Imbard, and C. Lévy (1998), OPA8.1 Ocean General Circulation Model reference manual, *Note du Pôle de modelisation, Institut Pierre-Simon Laplace (IPSL), France*, p. 91 pp.

Mahadevan, A., A. Tagliabue, L. Bopp, A. Lenton, L. Mémery, and M. Lévy (2011), Impact of episodic vertical fluxes on sea surface pCO_2, *Philos. Trans. R. Soc. A*, *369*, 2009–2025.

Marshall, G. J. (2003), Trends in the Southern Annular Mode from observations and reanalyses, *J. Clim.*, *16*, 4134–4143.

Marshall, G. J., P. A. Stott, J. Turner, W. M. Connolley, J. C. King, and T. A. Lachlan-Cope (2004), Causes of exceptional atmospheric circulation changes in the Southern Hemisphere, *Geophys. Res. Lett.*, *31*, L14205, doi:10.1029/2004GL019952.

Meredith, M. P., A. C. N. Garabato, A. M. C. Hogg, and R. Farneti (2012), Sensitivity of the overturning circulation in the Southern Ocean to decadal changes in wind forcing, *J. Clim.*, *25*, 99–110.

Mikaloff-Fletcher, S., et al. (2007), Inverse estimates of the oceanic sources and sinks of natural CO_2 and the implied oceanic carbon transport, *Global Biogeochem. Cycles*, *21*, GB1010, doi:10.1029/2006GB002751.

Mikaloff-Fletcher, S. E., et al. (2006), Inverse estimates of anthropogenic CO_2 uptake, transport, and storage by the ocean, *Global Biogeochem. Cycles*, *20*, GB2002, doi:10.1029/2005GB002530.

Morrison, A. K., and A. M. Hogg (2013), On the relationship between Southern Ocean overturning and ACC transport, *J. Phys. Oceanogr.*, *43*, 140–148.

Orr, J. C., et al. (2001), Estimates of anthropogenic carbon uptake from four three-dimensional global ocean models, *Global Biogeochem. Cycles*, *15*(1), 43–60.

Orsi, A., T. III Whitworth, and J. W. Nowlin (1995), On the meridional extent and fronts of the Antarctic Circumpolar Current, *Deep Sea Res. Part II*, *42*, 641–673.

Sabine, C., et al. (2004), The ocean sink for anthropogenic CO_2, *Science*, *305*, 367–370.

Sallée, J.-B., K. Speer, and R. Morrow (2008), Response of the Antarctic circumpolar current to atmospheric variability, *J. Clim.*, *21*, 3020–3039.

Sarmiento, J. L., and N. Gruber (2006), *Ocean Biogeochemical Dynamics*, Princeton Univ. Press, Princeton, N.J.

Sarmiento, J. L., J. C. Orr, and U. Siegenthaler (1992), A perturbation simulation of CO_2 uptake in an ocean general circulation modeling, *J. Geophys. Res.*, *97*, 3621–3645.

Sen Gupta, A., and M. H. England (2006), Coupled ocean-atmosphere-ice response to variations in the southern annular mode, *J. Clim.*, *19*, 4457–4486.

Spence, P., J. C. Fyfe, A. Montenegro, and A. J. Weaver (2010), Southern Ocean response to strengthening winds in an eddy-permitting global climate model, *J. Clim.*, *23*, 5332–5343.

Takahashi, T., J. Olafsson, J. G. Goddard, D. W. Chipman, and S. C. Sutherland (1993), Seasonal variation of CO_2 and nutrients in the high-latitude surface oceans: A comparative study, *Global Biogeochem. Cycles*, *7*(4), 843–878.

Takahashi, T., C. Sweeney, B. Hales, D. W. Chipman, T. Newberger, J. G. Goddard, R. A. Iannuzzi, and S. C. Sutherland (2012), The changing carbon cycle in the Southern Ocean, *Oceanography*, *25*(3), 26–37.

Talley, L. D. (2003), Shallow, intermediate, and deep overturning components of the global heat budget, *J. Phys. Oceanogr.*, *33*, 530–560.

Thompson, D. W. J., S. Solomon, P. J. Kushner, M. H. England, K. M. Grise, and D. J. Karoly (2011), Signatures of the Antarctic ozone hole in Southern Hemisphere surface climate change, *Nat. Geosci.*, *4*, 741–749.

Treguier, A.-M., M. H. England, S. R. Rintoul, G. Madec, J. Le Sommer, and J.-M. Molines (2007), Southern Ocean overturning across streamlines in an eddying simulation of the Antarctic Circumpolar Current, *Ocean Sci.*, *3*, 491–507.

Vialard, J., and P. Delecluse (1998), An OGCM study for the TOGA decade. Part I : Role of salinity in the physics of the Western Pacific fresh pool, *J. Phys. Oceanogr.*, *28*, 1071–1088.

Wanninkhof, R. (1992), Relationship between wind speed and gas exchange over the ocean, *J. Geophys. Res.*, *97*(C5), 7373–7382.

Weiss, R. F., and B. Price (1980), Nitrous oxide solubility in water and seawater, *Mar. Chem.*, *8*, 347–359.

Wetzel, P., A. Winguth, and E. Maier-Reimer (2005), Sea-to-air CO_2 flux from 1948 to 2003: A model study, *Global Biogeochem. Cycles*, *19*, GB2005, doi:10.1029/2004GB002339.

Whitworth, T. (1983), Monitoring the transport of the Antarctic circumpolar current at drake passage, *J. Phys. Oceanogr.*, *13*, 2045–2057.